Biosynthesis, characterization and antimicrobial activities of zinc oxide nanoparticles from leaf & seed extracts of *Malva neglecta* Wallr.

Abdol-Majid Cheperli
Majid Mokaber-Esfahani (m_mokaber@gonbad.ac.ir)
Gonbad Kavous University https://orcid.org/0000-0002-2128-719X
Akram Taleghani
Farhad bahalkeh

Research Article

Keywords: Malva neglecta Wallr, ZnO nanoparticles, Green fabricated, Antibacterial, Antioxidant, Extract

Posted Date: January 31st, 2022

DOI: https://doi.org/10.21203/rs.3.rs-1286975/v1

Abstract

Plant-based nanoparticles have a number of benefits over traditional physicochemical approaches, and they may be used in a variety of medical and biological applications. In recent study, a green synthesis approach for zinc oxide nanoparticles (ZnO NPs) using *Malva neglecta* Wallr. leaf (MWL) and seed (MWS) aqueous extracts were reported. MWL mediated ZnO NPs (MWL-ZnO-NPs) and MWS mediated ZnO NPs (MWS-ZnO-NPs) were synthesized using an environmentally friendly and simple technique with minimal reaction time and calcination temperature. The structural and chemical characterization of the biosynthesized ZnO NPs was performed using UV-Vis, FTIR, XRD, TGA, TEM, and EDX. Synthesized nanoparticles showed the UV–Visible spectroscopy absorption peak at 372 and 376 nm for MWL and MWS-ZnO-NPs, respectively, which confirm the synthesis of ZnO NPs. Furthermore, the FTIR spectrum indicated bioactive functional groups and metal-oxygen groups. The TEM analysis displayed that two different synthesized ZnO NPs, exhibited a somewhat spherical structure with an average particle size between 40 and 50 nm, regardless of the type of extract. EDX analysis approved the Zn and O in the synthesized ZnO NPs. The XRD results revealed that MWL-ZnO-NPs had a similar crystal structure to MWS-ZnO-NPs. The dose-dependent free radical scavenging capability of zinc oxide nanoparticles was determined using the 2,2-diphenyl-1-picryl-hydrazyl-hydrate (DPPH) test. Furthermore, the antibacterial activity of ZnO NPs was investigated using the paper disc diffusion technique against two clinical strains of Escherichia coli and Staphylococcus aureus using the zone of inhibition and minimum inhibitory concentration (MIC).

1. Introduction

In recent years, nanotechnology has attracted much attention due to its wide applications in various scientific fields such as chemistry, molecular biology, energy storage, micro fibrillation, pharmaceuticals, and optics. [1] Various nanoparticles (NPs) owing to their unique and fascinating physical and chemical properties, have a variety of uses in different areas, such as medicine, pharmaceuticals, cosmetics, food, energy, environmental, catalytic, and material applications. [2, 3] Among the available large number of nanoparticles, metal oxide nanoparticles attracted a great deal of researchers' attention due to their enormous potential across a broad range of research disciplines. [4] Zinc oxide nanoparticles (ZnO-NPs) are considered the most significant between the metal oxides NPs for their biocompatibility, high UV protection [5], low cost, non-toxicity, low electric resistance [6], thermal stability [7], and robustness [8]. So, these nanostructures are widely used in various fields such as the food industry [9], agriculture, solar cell [10], gas sensors [11], cosmetics [12], environmental remediation [13], and finally in medical fields such as gene delivery, wound healing [14], bio-imaging, drug delivery, biomedicine, especially in the fields of anticancer, antibacterial [15], anti-inflammatory, antioxidant, antifungal, and antidiabetic fields [16].

ZnO nanostructures have been fabricated using a variety of physical and chemical techniques such as thermal evaporation [17], pulsed laser deposition [18], sputtering [19], physical vapor deposition [20], precipitation [21], solvothermal [22], hydrolysis [23], hydrothermal [24], sol-gel, sonochemical, microwave, spray pyrolysis [25], etc. Though the synthesis of ZnO nanoparticles using these approaches is

successful. It requires high-cost equipments, harsh experimental conditions, hazardous chemicals, toxic reducing agents, and stabilizers [26] that are highly reactive and dangerous to the environment and living systems.

Therefore, to mitigate these problems, green processes can be used to synthesize ZnO nanoparticles. Less hazardous, safe [27], biocompatibility [28], eco-friendly [29], easily scaled up, energy-efficient, and cost-effective [15] are some of the advantages of these methods. Plants, fungi, bacteria, algae [30] are commonly used for the green synthesis of ZnO nanoparticles. Plant-derived products have recently gained significant popularity because of their low cost and less use of toxic chemicals [10]. Natural plant extracts are rich in phytochemicals such as tannins, amino acids, polyphenols, polysaccharides, terpenoids, flavonoids, and alkaloids, which act as strongly reduce and capping agents and lead to the synthesis of stabilized ZnO NPs [31]. Redox reaction occurs in the solution, and the extracts facilitate the electron transfer to the zinc ions to produce ZnO nanoparticles [8]. ZnO nanoparticles have been synthesized using various plant sources such as *Punica granatum* leaf [32], *Silybum marianum L.* seed [33], *Mentha pulegium L.* leaf [34], *Solanum nigrum* leaf [35], *Maple* leaf [36], *Berberis vulgaris* [37], *Hibiscus sabdariffa* [38], *Calotropis gigantean* [39], *Nigella sativa* seed [40], *Monsonia burkeana* [41] and *Camellia sinensis* [42].

M. neglecta Wallr. is a herbaceous plant of the *Malva* genus that goes by the names common mallow, dwarf mallow, cheese plant, cheese weed, buttonweed, and round leaf mallow [43]. The genus *Malva* is distributed throughout the subtropical, tropical and temperate zones of Europe, Asia, and Africa [44]. The leaves and roots of *M. neglecta* have traditionally been used as a salve for wound healing [45], inflammation, bruising, and insect bites, as well as internally for respiratory and urinary tract infections [46]. Various studies reveal the antioxidant [45], antibacterial [47], and anti-ulcerogenic [48] effects of this plant. It is also used to treat several diseases such as asthma, colds, digestive and urinary problems, and abdominal pain [49]. Accordingly, in this work, a green approach has been adopted to synthesize ZnO nanoparticles using *M. neglecta* leaf & seed aqueous extracts as reducing agents. Moreover, the antioxidant activity and antibacterial efficiency of synthesized MWL-ZnO-NPs and MWS-ZnO-NPs were evaluated against *Staphylococcus aureus* (*S. aureus*) and *Escherichia coli (E. coli).*

2. Materials And Methods

2.1 material

All chemicals and solvents were obtained from Sigma-Aldrich and were used without further purification. Distilled water was utilized in all experiments. *M. neglecta* was collected from Gonbad Kavous, Golestan province, Iran. Plant identification was performed by an expert of the plant systematic center of Gonbad Kavous University (herbarium number GKU/NO. 804117). The collected leaves and seeds were separately washed with distilled water to remove any contamination, shade dried for 4 days, crushed to powder using a spice grinder, and sieved through 60 Mesh. To avoid oxidation and humidity, the powder was kept

dry in airtight containers. The bacterial species *S. aureus* (ATCC 9144) and *E. coli* (ATCC 25922) were provided from the Persian Type Culture Collection, Tehran, Iran (PTCC).

2.2. Green synthesis of ZnO nanoparticles

2.2.1 Preparation of M. neglecta seed & leaf extract

To prepare the MWL and MWS aqueous extracts, 2 g of seed and leaf powder were poured separately in 100 mL of distilled water and heated at 90 °C for 3 hours. The resulting mixture was stirred at room temperature for 1 hour. After filtration using Whatman No. 1 paper, the extract was stored at 4°C for subsequent research.

2.2.2 Green synthesis of ZnO NPs

A solution of $Zn(NO_3)_2 \cdot 6H_2O$ (2 gr) in 3 mL deionized water was added dropwise to 45 mL of MWL and MWS extracts, separately. The resulting mixtures were stirred at room temperature for 1 hour. These mixtures were heated continuously at 60 °C for an hour on a magnetic stirrer hotplate. Afterward, the mixtures were dried in the oven at 150°C. Finally, the as-synthesized samples were calcined for 4 hours at 400°C in a muffle furnace. The resulting products were stored in airtight bottles for further analysis. High product yields of 31.2 and 29.8% (w/w) were obtained for the MWL and MWS ZnO-NPs. MWL and MWS extracts are used to synthesize ZnO nanoparticles depicted in Fig. 1.

2.3 Characterizations of green synthesized nanostructured ZnO

Confirmation of nanoparticle synthesis was obtained using a UV-Vis spectrophotometer (Shimadzu). Fourier-transform infrared spectra were recorded on an FTIR spectrophotometer (Perkin Elmer, USA). X-ray diffraction (XRD) patterns of the samples were obtained using X-Ray Diffraction Equipment (PANalytical X'Pert Pro MRD). The thermal behavior of the samples was studied by Thermogravimetric Analysis (TGA) equipment (STA 504, TA Instrument). The analysis of the elemental composition of samples was recorded by using energy dispersive X-ray (FE-SEM, UK). TEM images were obtained on a Philips EM208 microscope (Phillips, Eindhoven, Netherlands) with an accelerating voltage of 100 kV. The average particle size of each sample was obtained using ImageJ software.

2.4 Phytochemical analysis: total phenolic (TPC) and total flavonoid contents (TFC).

To get total phenolic content (TPC), Folin–Ciocalteu reagent was used with some modifications, and it was expressed as mg of gallic acid (GAE) per gram of dry weight (mg/g) [50]. The mixture consisted of 20 µL of extract solution (2% w/v), 100 µL Folin–Ciocalteu reagent, and 1.16 mL water was mixed for 8 min. Then 300 µL sodium carbonate (Na_2CO_3 20% w/v) was added and incubated at 40°C for 30 min. A

spectrophotometer measured the absorbance of the samples in comparison to a prepared blank at a wavelength of 765 nm. Finally, gallic acid is employed as a reference material.

A standard curve (Y = 0.0086X - 0.0104) from the gallic acid with concentrations of 10-100 µg/mL have been calculated.

TFC might be measured using an aluminum chloride colorimetric technique [51]. 0.5 mL of each extract was added to 1.5 mL of 95% alcohol, 0.1 mL of aluminum chloride (10%), 0.1 mL of potassium acetate 1M and 2.8 mL of water. The mixture was incubated at room temperature for 30 minutes. The blank was used to measure the mixture's absorbance at 415 nm. The TFC was measured using quercetin standard curves (Y = 0.0071X + 0.0338) and reported as mg quercetin (QE) per gram of dry weight (mg/g).

2.5 Antioxidant activity using DPPH assay

MWL-ZnO-NPs and MWS-ZnO-NPs antioxidant activity was determined using the DPPH method, as previously described by Sohail et al. [14], with some modifications. The DPPH free radical scavenging assay was used to determine the antioxidant activity of MWL-ZnO-NPs and MWS-ZnO-NPs. Briefly, 200 µL of various concentrations of the samples (15.62-250 µg/mL) were added to 1.8 mL of methanolic solution of DPPH (0.1 mM) and was shaken vigorously. The reaction mixtures were incubated in the dark at room temperature for 1 hour, then the absorbance of each sample was determined at 517 nm. DPPH solution was used as positive controls. The free radical scavenging activity of each sample was determined using the following equation:

$$Antioxidantactivity = \frac{Abs(control) - Abs(sample)}{Abs(control)} \times 100$$

2.6 Antibacterial assay

The bacterial growth inhibitory activity of MWL-ZnO-NPs and MWS-ZnO-NPs were measured using broth dilution and agar disc diffusion methods.

2.6.1 Broth dilution method

The minimum inhibitory concentration (MIC) and minimum bactericidal concentration (MBC) were calculated using a broth dilution method in accordance with Clinical & Laboratory Standards Institute (CLSI) guidelines [52]. Briefly, serial dilutions of MWL-ZnO and MWS-ZnO nanoparticles (500, 250, 125, 62.5, 31.25, 15.62 µg/mL) were prepared in 2 mL of nutrient broth culture medium. The green synthesized ZnO-NPs suspension (200 µL) was inoculated with the microbial suspension (100 µL) at 37°C for 24 h. As negative and positive controls, tubes containing growth media alone or bacterial culture without ZnO nanoparticle suspensions were utilized. After 24 hours of incubation, the lowest dose at which no visible bacteria grow was determined to be the MIC. Subsequently, for the MBC test, 100 µl of broth from each test tube that did not show growth was inoculated in a nutrient agar plate at 37°C for 24 h. The lowest concentration of ZnO nanoparticles that bacteria did not grow was reported as the minimum bactericidal concentration.

2.6.2 Antibacterial screening by agar disc diffusion method

In-vitro disc diffusion method [53] was used to evaluate the bactericidal ability of green synthesized zinc oxide nanoparticles. Petri dishes containing 10 mL of nutrient agar were inoculated with 100 µL of the bacterial suspension. After inoculating the plates, they were allowed to dry for 20 minutes. Green synthesized ZnO-NPs solutions at concentrations of 62.5, 125, 250, and 500 µg/mL were loaded onto sterile discs 6 mm in diameter. Negative controls included a blank disc impregnated with solvent (0.9% NaCl solution), while positive controls included tetracycline (5 µg/disc). During the first hour at room temperature, the green nanostructured ZnO was allowed to diffuse across the surface, and then the plates were incubated at 37°C for 24 hours. Finally, to determine the antibacterial activity of the ZnO-NPs and controls, we measured the clear zones of inhibition surrounding each disc and recorded the result in millimeters. In each case, sterilized forceps were used to place discs containing various fractions on the inoculated plates carefully and gently pressed against the agar to ensure contact.

2.6. Statistical analysis

The data were statistically analyzed using a two-way analysis of variance (ANOVA). The results were expressed as mean ± SD.

3. Results And Discussion

3.1 Characterization of the ZnO nanoparticle

3.1.1 UV–Visible spectroscopic analysis

The UV-Vis absorption of biosynthesized ZnO nanoparticles is presented in Fig. 2. The MWL-ZnO-NPs and MWS-ZnO-NPs annealed at 400°C showed a strong absorption band at 372 and 376 nm, respectively. The obtained results demonstrated good agreement with the previously reported literature on green synthesized ZnO NPs [54], they confirmed the formation of biosynthesized ZnO nanoparticles.

3.1.2. Fourier-transform infrared (FTIR) spectroscopy

MWL-ZnO-NPs, MWS-ZnO-NPs, as-prepared samples, MWL, and MWS extracts were recognized using FTIR spectroscopy. As illustrated in Fig. 3, the FTIR spectrum of MWL and MWS extracts a broad peak at around 3400 cm^{-1} attributed to the stretching vibrations of OH and $-NH_2$ functional groups of the polyols. Moreover, the stretching vibrations of C=C and C=O bonds on the aromatic rings of the phenolic compounds were observed at around 1400 and 1600 cm^{-1}, respectively [55]. The peak at about 1100 cm^{-1} represented the stretching vibration of the hydroxyl C-O bond of flavonoids and phenolic compounds. The FTIR spectra of biosynthesized ZnO nanoparticles for samples annealed at 400°C revealed additional absorption peaks between 440 and 500 cm^{-1} corresponding to the stretching vibration of Zn–O bonding, confirming the creation of ZnO nanoparticles. Furthermore, the peak at around 3400 cm^{-1} corresponds to OH vibrations caused by the hydrogen bond interaction of ZnO nanoparticles with water. [56]. It is noteworthy that the FTIR spectrum of ZnO nanoparticles exhibited

several peaks at the same position of the FTIR spectrum of the extracts. This may be due to the low annealing temperature of ZnO nanoparticles, which does not allow complete decomposition of organic compounds. As illustrated in Fig. 3, there is some blue shift of typical peaks at around 1100, 1400, and 1600 cm^{-1} for ZnO NPs that confirm the interaction of the phenolic compounds with the surface of the MWL-ZnO and MWS-ZnO NPs [57, 55].

3.1.1 Transmission Electron Microscopy (TEM) & Energy Dispersive X-Ray (EDX) analysis

The morphology and particle size of MWL-ZnO-NPs and MWS-ZnO-NPs annealed at 400°C were characterized using TEM analysis. Both MWL and MWS-ZnO-NPs samples represented somewhat spherical shape morphology and were aggregated to some extent, as revealed in Fig. 4(a). The particle size distribution curve for the green synthesized zinc oxide nanoparticles are represented in Fig. 4(b). The mean particle size was 40.46±7.25 and 46.60±11.90 nm for the ZnO NPs synthesized by MWL and MWS extract, respectively. As shown by the results, MWL extract is slightly more effective for the synthesis of smaller ZnO-NPs than MWS extract. Due to polycrystalline aggregation, the particle sizes of MWL-ZnO and MWS-ZnO nanoparticles were greater than their crystal sizes predicted from XRD profiles [58]. Energy Dispersive X-Ray (EDX) spectroscopy was used to determine the compositional analysis of biosynthesized ZnO nanoparticles. As depicted in Fig. 5, the Zn Kα, Zn Lα, Zn Kβ and O Kα were observed in the EDX spectrum for both NPs, thereby confirming the green synthesis of MWL-ZnO-NPs and MWS-ZnO-NPs. The weight percentage of zinc and oxygen elements were received in 72.08, 20.50%, for MWL-ZnO-NPs, and 62.64, 25.64% for MWS-ZnO-NPs, respectively. There is also some weak signal and weight loss, which could be related to the plant compounds used for the biosynthesis of ZnO nanoparticles.

3.1.3 X-ray diffraction (XRD) analysis of ZnO NPs

Figure 6 illustrates the X-ray diffraction (XRD) patterns of the as-prepared and ZnO-NPs. As can be seen, the as-prepared sample lacked crystal structure as a result of the low-temperature synthesis. While, in the XRD pattern of green synthesized ZnO nanoparticles, the sharp peaks with a definite line broadening displayed the synthesized ZnO particles in the nano-scale range. MWL-ZnO-NPs showed strong diffraction peaks at 31.80, 34.45, 36.29, 47.56, 56.60, 62.91, 66.54, 67.96, 69.06, 72.43, 77.09, and 81.38. While MWS-ZnO-NPs had strong diffraction peaks at 31.89, 34.55, 36.36, 47.64, 56.67, 62.99, 66.54, 68.05, 69.20, 72.72, 76.95, and 81.49. All the biosynthesized ZnO nanoparticles diffraction peaks corresponded to the crystallographic (100), (002), (101), (102), (110), (103), (200), (112), (201), (004), (202), and (104) planes respectively. Notably, the XRD pattern of the synthesized NPs is highly compatible with the wurtzite hexagonal structure of ZnO [59]. The obtained pattern was consistent with JCPDS card no. 01-089-0510 and 01-075-0576 for MWL-ZnO-NPs and MWS-ZnO-NPs, respectively. Furthermore, using the Debye–Scherrer equation, the crystallite size of the MWL-ZnO-NPs and MWS-ZnO-NPs was determined to be 34.2 and 42.2 nm, respectively, from the diffractogram's high-intensity peak at (101) plane [60]. Consequently, by comparing the XRD results of the MWL-ZnO-NPs and MWS-ZnO-NPs, it was found that the natural resources used in the fabrication of nanoparticles might have a greater impact

on the size of the ZnO nanoparticles than their crystal structure. [31] The crystallite size determined by XRD analysis is consistent with the particle size distribution calculated from TEM analysis.

3.1.4 Thermogravimetry analysis (TGA)

Thermogravimetry diagram of the synthesized as-prepared ZnO samples and ZnO NPs in Fig. 7. Compared with the as-prepared sample, the MWL-ZnO-NPs and MWS-ZnO-NPs samples exhibited nearly no weight loss. For the as-prepared sample, the thermogram showed two distinctive regions of weight losses. At 100 ^{o}C, weight loss was detected as a result of moisture and volatiles evaporating from the particles' surfaces. The remaining precursors are eliminated and emitted as CO_2 between 100 and 400 ^{o}C. At 400 ^{o}C, the weight loss appeared to stabilize, indicating that the majority of organic contaminants had been eliminated. Weight loss was minimal in the annealed samples, owing primarily to moisture and CO_2 absorption [25].

3.2 Total phenol and flavonoid contents.

The antioxidant activity of phenolic extracts is correlated with the TPC and TFC. They reduce and stabilize metal ions during the production of metal nanoparticles [61, 62]. The TPC and TFC levels in *M. neglecta* seed and leaf extracts were determined using the Folin–Ciocalteu reagent and the aluminum chloride colorimetric method, respectively. The values for total phenol and flavonoid are shown in Table 1. Seed and leaf extracts contain sufficient amounts of phenolic and flavonoid compounds. The TPC value was higher in the leaf extract (202.8±3.52 mg GAE/g) than the seed extract (109.9±2.79 mg GAE/g). Also, TFC values were 28.27±2. mg QE/g and 21.1±2.14 mg QE/g for seed and leaf extracts, respectively. The formation of ZnO nanoparticles may be influenced by various biomolecules in aqueous plant extracts, including polyphenols and flavonoids. Also, high levels of total phenols in these extracts are responsible for their high antioxidant capacity [63].

Table 1
The TPC and TFC of seed and leaf extracts of *M. neglecta.*

	Plant part	Total phenols mg GAE/g DW	Total flavonoids mg quercetin/g DW
M. neglecta	Seed extract	109.9±2.79	28.27±2.01
	Leaf extract	202.8±3.52	21.1±2.14

GA: Gallic acid, DW: dried weight. All data represented the mean ± standard deviation of three independent experiments.

3.3 Antioxidant Activity

DPPH radical scavenging assay was used to determine the antioxidant activity of the green synthesized ZnO NPs. As shown in Fig. 8, at concentrations of 15.62-250 µg/mL, the MWS-ZnO-NPs and MWL-ZnO-

NPs had antioxidant activity between 22.39±1.53% to 49.08±1.90% and 23.59±1.18% to 55.33±2.30%, respectively. The results reveal that with increasing the concentration of ZnO-NPs, the absorption of DPPH radicals increased and a maximum of 55.33% was observed at 250 µg/mL. The results indicate that ZnO-NPs are effective inhibitors of reactive oxygen species with a wide range of activity.

3.4 Antibacterial activity

The antibacterial activity of biosynthesized ZnO-NPs against pathogenic gram-positive (*S. aureus*) and gram-negative (*E. coli*) bacteria was initially determined using two assays, disc diffusion and MIC-MBC. Zones of inhibition of *E. coli* and *S. aureus* by standard drugs, MWL-ZnO-NPs, and MWS-ZnO-NPs at concentrations ranging from 62.5 to 500 µg/mL are depicted in Fig. 9. Table 2 shows the mean values of the zone of inhibition (mm) for three replicates. MWL-ZnO-NPs and MWS-ZnO-NPs shown moderate antibacterial effectiveness against both gram-positive and gram-negative bacteria when compared to standard antibiotics (Tetracycline). No single dose has shown more substantial potential than the positive control. Statistical analysis showed no significant difference between the antibacterial effects of green synthesized ZnO nanoparticles on the studied bacterial strains. Furthermore, the natural resources (*M. neglecta* leaf & seed) don't have a significant influence on the bactericidal activity of the ZnO NPs toward *E. coli* and *S. aureus*. The antibacterial activity also significantly increased with increasing concentrations of biosynthesized ZnO-NPs, and the maximum inhibitory zone was observed at 500 µg/mL of MWS-ZnO-NPs and MWL-ZnO-NPs for both strains *S. aureus* and *E. coli*. This was in agreement with previous studies where ZnO nanoparticle activity was dose-dependent [64].

MWS-ZnO-NPs and MWL-ZnO-NPs were tested for bacteriostatic and bactericidal effects using the MIC-MBC method at concentrations of 15.62, 31.25, 62.5, 125, 250, 500, and 1000 µg/mL. According to Table 3, the MIC-MBC assay values were consistent with the disc diffusion assay results. MWL-ZnO-NPs and MWS-ZnO-NPs had MIC values of 31.25 µg/L and 62.5 µg/L, respectively, against *E. coli* and *S. aureus*. In addition, MBC values of 125 and 62.5 µg/ mL were observed for MWS-ZnO-NPs and MWL-ZnO-NPs, respectively, against both *E. coli* and *S. aureus*.

In accordance with the results of Zhang et al. [65], the bactericidal ability of ZnO nanoparticles is due to reactive oxygen species (ROS). As ZnO NPs interact with the bacterial membrane or enter through bacterial transport channels, they release ROS, predominantly H_2O_2, OH°, and O_2^- radicals, damaging the bacterial DNA and cell walls. In addition, zinc oxide nanoparticles have a surface zeta potential. This makes it easier to adhere to bacteria's surfaces. Zinc oxide inhibits bacterial growth by causing damage to the cell membrane or extrusion of cytoplasmic content [66].

Table 2
Antibacterial assessment of the biosynthetic ZnO-NPs.

Bacterial species		Concentration (µg/mL) of ZnO NPs				Blank disc (-ve control)	Tetracycline (+ve control)
		500	250	125	62.5		
E. coli	seed	12.35±0.08	10.82±0.09	9.53±0.07	No zone	No zone	19.46±0.26
	leaf	12.40±0.15	11.00±0.28	9.66±0.08	No zone	No zone	19.46±0.26
S. aureus	seed	12.30±0.28	10.90±0.15	9.62±0.09	No zone	No zone	19.49±0.08
	leaf	12.42±0.18	10.95±0.35	9.85±0.21	No zone	No zone	19.49±0.08

Zones of inhibition (mm) are presented as mean ± SD.

Table 3
MIC and MBC of MWL and MWS-ZnO-NPs against *E. coli* and *S. aureus*.

Bacterial species		MIC (µg/mL)	MBC (µg/mL)
E. coli	seed	62.5	125
	leaf	31.25	62.5
S. aureus	seed	62.5	125
	leaf	31.25	62.5

4. Conclusion

We effectively produced ZnO nanoparticles in this study by employing aqueous extracts of *M. neglecta* leaf and seed as a reducing agent in an environmentally safe and green method. The UV-Visible spectrum confirms the synthesis of ZnO NPs. The FTIR spectrum indicated bioactive functional groups and metal-oxygen groups. TEM analysis displayed a somewhat spherical structure with an average particle size of 40.46 and 46.60 nm for the ZnO NPs synthesized by MWL and MWS extract, respectively. Both extracts formed ZnO NPs with similar crystal structures, as shown by XRD. Also, the capacity of zinc oxide nanoparticles to scavenge free radicals was comparable. We found that the natural resources (*M. neglecta* leaf & seed) had no significant effect on the microstructural characteristics, antioxidant capacity, and bactericidal activity of ZnO NPs against *E. coli* and *S. aureus*. The results reveal that both types of synthesized zinc oxide nanoparticles could be effective in biological applications.

Declarations

Acknowledgments

Authors thanks Gonbad Kavous University for the financial and facilitation support of this work.

- The authors declare that they have no known competing financial interests or personal relationships that could have appeared to influence the work reported in this paper.
- All authors contributed to the study conception and design. Material preparation, data collection and analysis were performed by Majid Mokaber-Esfahani, Abdol-Majid Cheperli, Akram Taleghani, and Farhad Bahalkeh. The first draft of the manuscript was written by Majid Mokaber-Esfahani and all authors commented on previous versions of the manuscript. All authors read and approved the final manuscript.

References

1. M.N. Nadagouda, N. Iyanna, J. Lalley, H. Changseok, D.D. Dionysiou, R.S. Varma, ACS Sustain. Chem. Eng. **2**(7), 1717–1723 (2014)
2. J. Lu, H. Ali, J. Hurh, Y. Han, I. Batjikh, E.J. Rupa, G. Anandapadmanaban, J.K. Park, D.C. Yang, Optik **184**, 82–89 (2019)
3. B.A. Abbasi, J. Iqbal, T. Mahmood, R. Ahmad, S. Kanwal, S. Afridi, Mater. Res. Express **6**(8), 0850a7 (2019)
4. B. Baruwati, V. Polshettiwar, R.S. Varma, Green Chem. **11**, 926–930 (2009)
5. L.H. Zhao, R. Zhang, J. Zhanga, S.Q. Sun, CrystEngComm **14**, 945–950 (2012)
6. B. Şahin, S. Soylu, M. Kara, M. Türkmen, R. Aydin, H. Çetin, Ceram. Int. **47**, 341–350 (2021)
7. A.K. Chauhan, N. Kataria, V.K. Garg, Chemosphere. **247**, 125803 (2020)
8. F.H. Abdullah, N.H.H. Abu Bakar, M. Abu Bakar, Optik **206**, 164279 (2020)
9. P.J.P. Espitia, N.D.F.F. Soares, J.S. dos Reis Coimbra, N.J. de Andrade, R.S. Cruz, E.A.A. Medeiros, Food Bioprocess Tech. **5**(5), 1447–1464 (2012)
10. H. Upadhyaya, S. Shome, R. Sarma, S. Tewari, M.K. Bhattacharya, S.K. Panda, Am. J. Plant Sci. **9**, 1279–1291 (2018)
11. V. Galstyan, E. Comini, C. Baratto, G. Faglia, G. Sberveglieri, Ceram. Int. **41**(10), 14239–14244 (2015)
12. A. Miri, M. Khatami, O. Ebrahimy, M. Sarani, Green Chem. Lett. Rev. **13**(1), 27–33 (2020)
13. S. Kumar, A. Kumar, A. Kumar, V. Krishnan, Catal. Rev. **62**(3), 346–405 (2020)
14. M.F. Sohail, M. Rehman, S.Z. Hussain, Z. Huma, G. Shahnaz, O.S. Qureshi, Q. Khalid, S. Mirza, I. Hussain, T.J. Webster, J. Drug. Deliv. Sci. Tec. **59**, 101911 (2020)
15. B.A. Abbasi, J. Iqbal, R. Ahmad, L. Zia, S. Kanwal, T. Mahmood, C. Wang, J.T. Chen, Biomolecules **10**(1), 38 (2020)
16. V. Vinotha, A. Iswarya, R. Thaya, M. Govindarajan, N.S. Alharbi, S. Kadaikunnan, J.M. Khaled, M.N. Al-Anbr, B. Vaseeharan, J. Photoch. Photobio. B **197**, 111541 (2019)
17. F.T. Thema, E. Manikandan, M.S. Dhlamini, M. Maaza, Mater. Lett. **161**, 124–127 (2015)

18. Z.E. Vakulov, E.G. Zamburg, D.A. Khakhulin, O.A. Ageev, Mat. Sci. Semicon. Proc. **66**, 21–25 (2017)
19. A.N. Reed, P.J. Shamberger, J.J. Hu, C. Muratore, J.E. Bultman, A.A. Voevodin, Thin Solid Films **579**, 30–37 (2015)
20. G. Sharmila, M. Thirumarimurugan, C. Muthukumaran, Microchem. J. **145**, 578–587 (2019)
21. L. Zhao, Y. Sun, J.A. Hernandez-Viezcas, A.D. Servin, J. Hong, G. Niu, J.R. Peralta-Videa, M. Duarte-Gardea, J.L. Gardea-Torresdey, J. Agr. Food Chem. **61**(49), 11945–11951 (2013)
22. M.M. Rashad, A.A. Ismail, I. Osama, I.A. Ibrahim, A.H.T. Kandil, Arab. J. Chem. **7**(1), 71–77 (2014)
23. S.T. Tan, C.H. Tan, W.Y. Chong, C.C. Yap, A.A. Umar, R.T. Ginting, H.B. Lee, K.S. Lim, M. Yahaya, M. Mat, Sensor Actuat. B-Chem. **227**, 304–312 (2016)
24. N. Ekthammathat, S. Thongtem, T. Thongtem, A. Phuruangrat, Powder Technol. **254**, 199–205 (2014)
25. T.U.D. Thi, T.T. Nguyen, Y.D. Thi, K.H.T. Thi, B.T. Phan, K.N. Pham, RSC Adv. **10**, 23899–23907 (2020)
26. M. Golmohammadi, M. Honarmand, S. Ghanbari, Spectrochim. Acta A **229**, 117961 (2020)
27. K. Velsankar, S. Sudhahar, G. Parvathy, R. Kaliammal, Mater. Chem. Phys. **239**, 121976 (2020)
28. A. Miri, M. Darroudi, M. Sarani, Appl. Organomet. Chem. **34**, e5308 (2020)
29. G. Shi, Y. Li, G. Xi, Q. Xu, Z. He, Y. Liu, J. Zhang, J. Cai, J. Hazard. Mater. **335**, 170–177 (2017)
30. N. Durán, P.D. Marcato, M. Durán, A. Yadav, A. Gade, M. Rai, Appl. Microbiol. Biot. **90**, 1609–1624 (2011)
31. Y. Gao, D. Xu, D. Ren, K. Zeng, X. Wu, LWT-Food Sci. Technol. **126**, 109297 (2020)
32. K. Singh, J. Singh, M. Rawat, SN Appl. Sci. 1(624), (2019)
33. F.M. Arvanag, A. Bayrami, A. Habibi-Yangjeh, S.R. Pouran, Mater. Sci. Eng. C **97**, 397–405 (2019)
34. S. Shahriyari Rad, A.M. Sani, S. Mohseni, Microb. Pathogenesis **131**, 239–245 (2019)
35. M. Ramesh, M. Anbuvannan, G. Viruthagiri, Spectrochim. Acta A **136**, 864–870 (2015)
36. S. Vivekandhan, M. Schereiber, C. Mason, A.K. Mohanty, M. Misra, Colloid Surface B. **113**, 169–175 (2014)
37. Y. Anzabi, Green Process. Synth. **7**, 114–121 (2018)
38. N. Bala, S. Saha, M. Chakraborty, M. Maiti, S. Das, R. Basu, P. Nandy, RSC Adv. **5**, 4993–5003 (2015)
39. S.K. Chaudhuri, L. Malodia, Appl. Nanosci. **7**, 501–512 (2017)
40. A. Alaghemand, S. Khaghani, M.R. Bihamta, M. Gomarian, M. Ghorbanpour. J. Nanostruct. **8**, 82–88 (2018)
41. N.M. Ngoepe, Z. Mbita, M. Mathipa, N. Mketoe, B. Ntsendwana, N.C. Hintsho-Mbita, Ceram. Int. **44**, 16999–17006 (2018)
42. M. Naseer, U. Aslam, B. Khalid, B. Chen, Sci. Rep. 10 (9055), (2020)
43. U. Saleem, S. Khalid, S. Zaib, F. Anwar, B. Ahmad, I. Ullah, A. Zeb, M. Ayaz, J. Ethnopharmacol. **249**, 112401 (2020)
44. A. Mavi, Z. Terzi, U. Ozgen, A. Yildirim, M. Coskun, Biol. Pharm. Bull. **27**(5), 702–705 (2004)

45. A. Dalar, M. Türker, I. Konczak, J. Herb. Med. **2**, 42–51 (2012)
46. S.M. Seyyednejad, H. Koochak, E. Darabpour, H. Motamedi, Asian Pac. J. Trop. Medicine **3**(5), 351–355 (2010)
47. A. Jafari-Sales, B. Jafari, J. Sayyahi, T. Zohoori-Bonab, J. Biol. Today's World **4**(2), 58–62 (2015)
48. I. Gürbüz, A.M. Ozkan, E. Yesilada, O. Kutsal, J. Ethnopharmacol. **101**, 313–318 (2005)
49. M. Türker, A. Dalar, Ind. Crop. Prod. **51**, 376–380 (2013)
50. E.A. Ainsworth, K.M. Gillespie, Nat. Protoc. **2**, 875–877 (2007)
51. C.C. Chang, M.H. Yang, H.M. Wen, J.C. Chern, J. Food Drug Anal. **10**(3), 178–182 (2002)
52. CLSI, Methods for Dilution Antimicrobial Susceptibility Tests for Bacteria that Grow Aerobically, 8th ed., Villanova, PA, USA, 2003
53. K. Elumalai, S. Velmurugan, Appl. Surf. Sci. **345**, 329–336 (2015)
54. A. Diallo, B.D. Ngom, E. Park, M. Maaza, J. Alloy. Compd. **646**, 425–430 (2015)
55. M.O. Kareem, A.A. Edathil, K. Rambabu, G. Bharath, F. Banat, G.S. Nirmala, K. Sathiyanarayanan, Chem. Eng. Commun. **208**, 801–811 (2019)
56. K. Vimala, S. Sundarraj, M. Paulpandi, S. Vengatesan, S. Kannan, Process Biochem. **49**(1), 160–172 (2014)
57. N. Matinise, X.G. Fuku, K. Kaviyarasu, N. Mayedwa, M. Maaza, Appl. Surf. Sci. **406**, 339–347 (2017)
58. M. Thirumavalavan, K.L. Huang, J.F. Lee, Colloid. Surface A **417**, 154–160 (2013).
59. Z. Li, Z. Zhou, G. Yun, K. Shi, X. Lv, B. Yang, Nanoscale. Res. Lett. **8**, 473 (2013)
60. B. Jaber, L. Laanab, Mat. Sci. Semicon. Proc. **27**, 446–451 (2014)
61. F.D. Pelle, M.C. González, M. Sergi, M.D. Carlo, D. Compagnone, A. Escarpa, Anal. Chem. **87**(13), 6905–6911 (2015)
62. A. Alirezalu, P. Salehi, N. Ahmadi, A. Sonboli, S. Aceto, H.H. Maleki, M. Ayyari, Int. J. Food Prop. **21**(1), 452–470 (2018)
63. S. Ullah, A. Ahmad, H. Ri, A.U. Khan, U.A. Khan, Q. Yuan, Appl. Organomet. Chem. **34**(1), e5298 (2019)
64. A.A. Mohamed, A. Fouda, M.A. Abdel-Rahman, S.E.D. Hassan, M.S. El-Gamal, S.S. Salem, T.I. Shaheen, Biocatal. Agric. Biotechnol. **19**, 101103 (2019)
65. L. Zhang, Y. Jiang, Y. Ding, N. Daskalakis, L. Jeuken, M. Povey, A.J. O'Neill, D.W. York, J. Nanopart. Res. **12**, 1625–1636 (2010)
66. S. Divyapriya, C. Sowmia, S. Sasikala, World J. Pharm. Pharm. Sci. **3**(12), 1635–1645 (2014)

Figures

Figure 1

Schematic diagram of the biosynthesis of ZnO nanoparticles using M. neglecta leaf and seed extract.

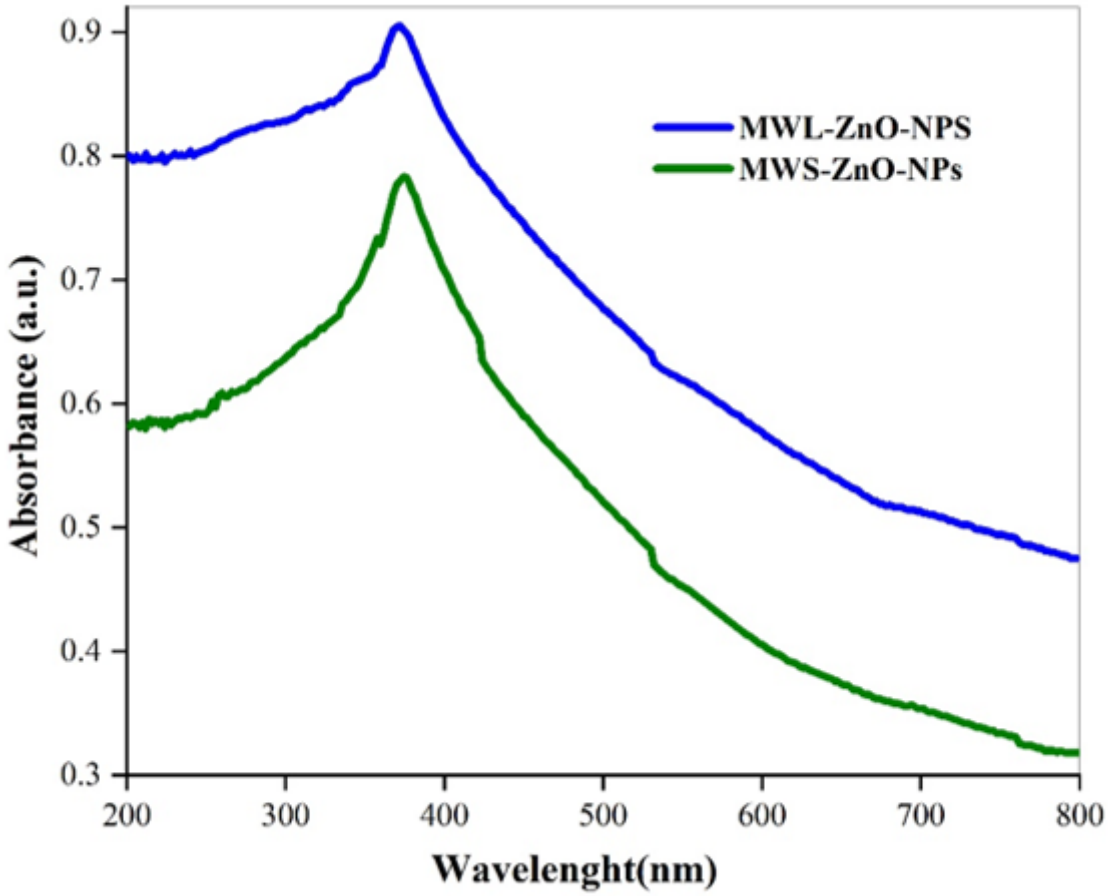

Figure 2

UV–Vis spectrum of ZnO nanoparticles.

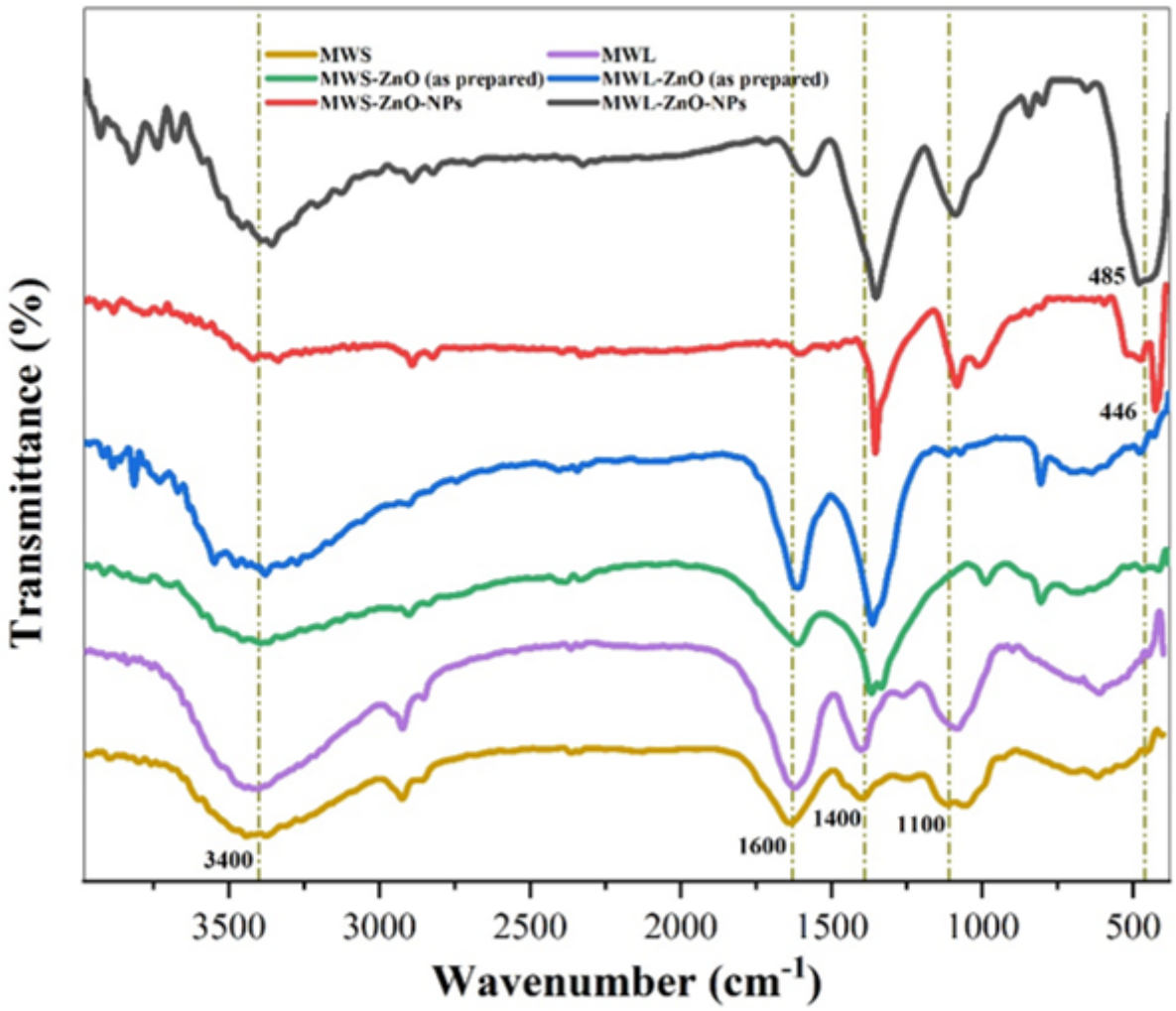

Figure 3

The Fourier-transform infrared spectra of MWL, MWS extract, as-prepared ZnO, and ZnO NPs.

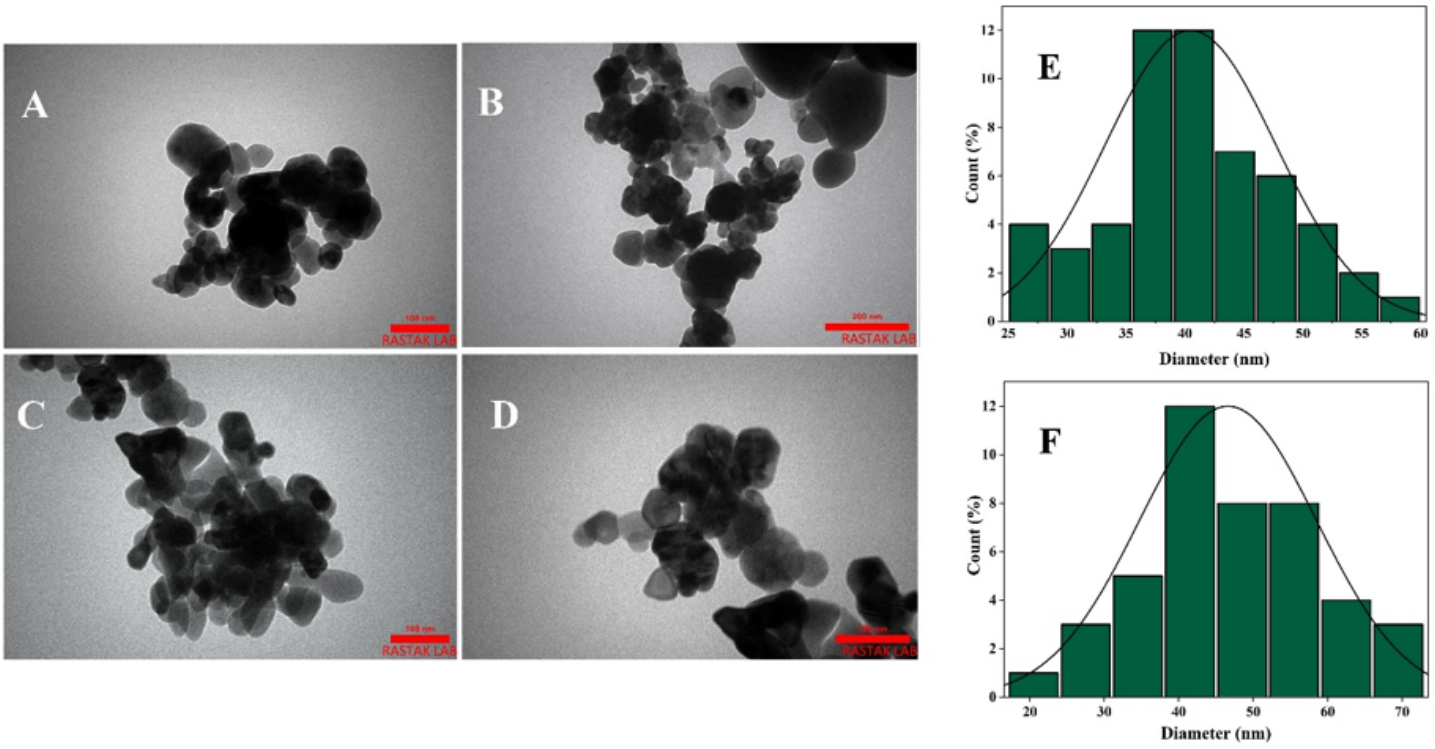

Figure 4

Transmission electron micrographs (TEM) of MWL mediated ZnO NPs (A, B) and MWS mediated ZnO NPs (C, D); Size distribution of particles in TEM images of MWL-ZnO-NPs (E), and MWS-ZnO-NPs (F).

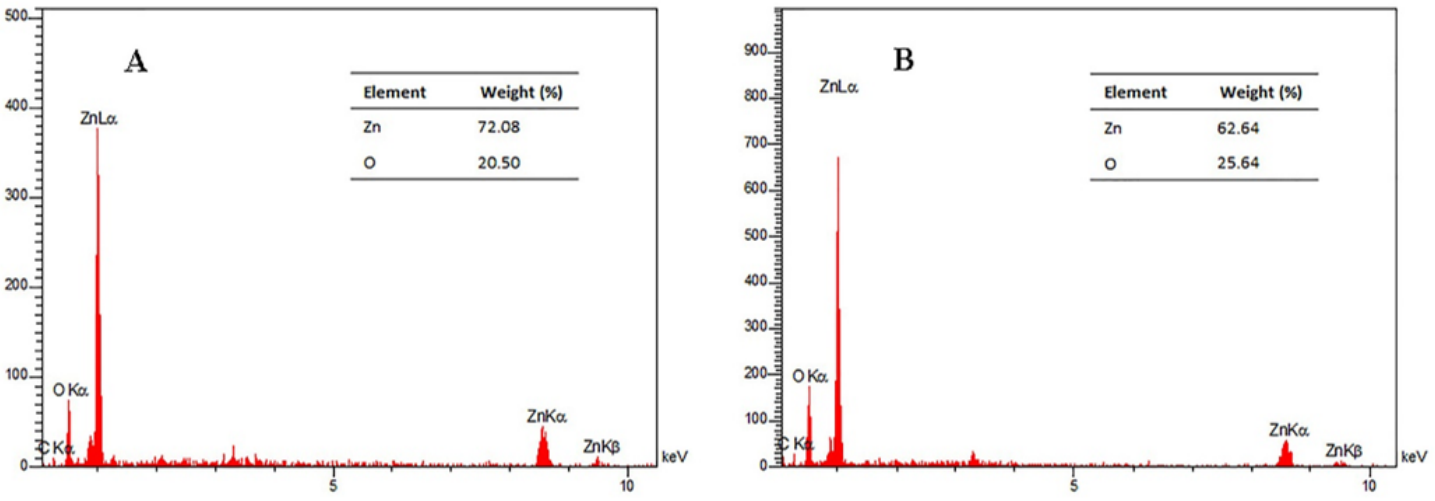

Figure 5

EDX spectra of MWL-ZnO-NPs (A) and MWS-ZnO-NPs (B).

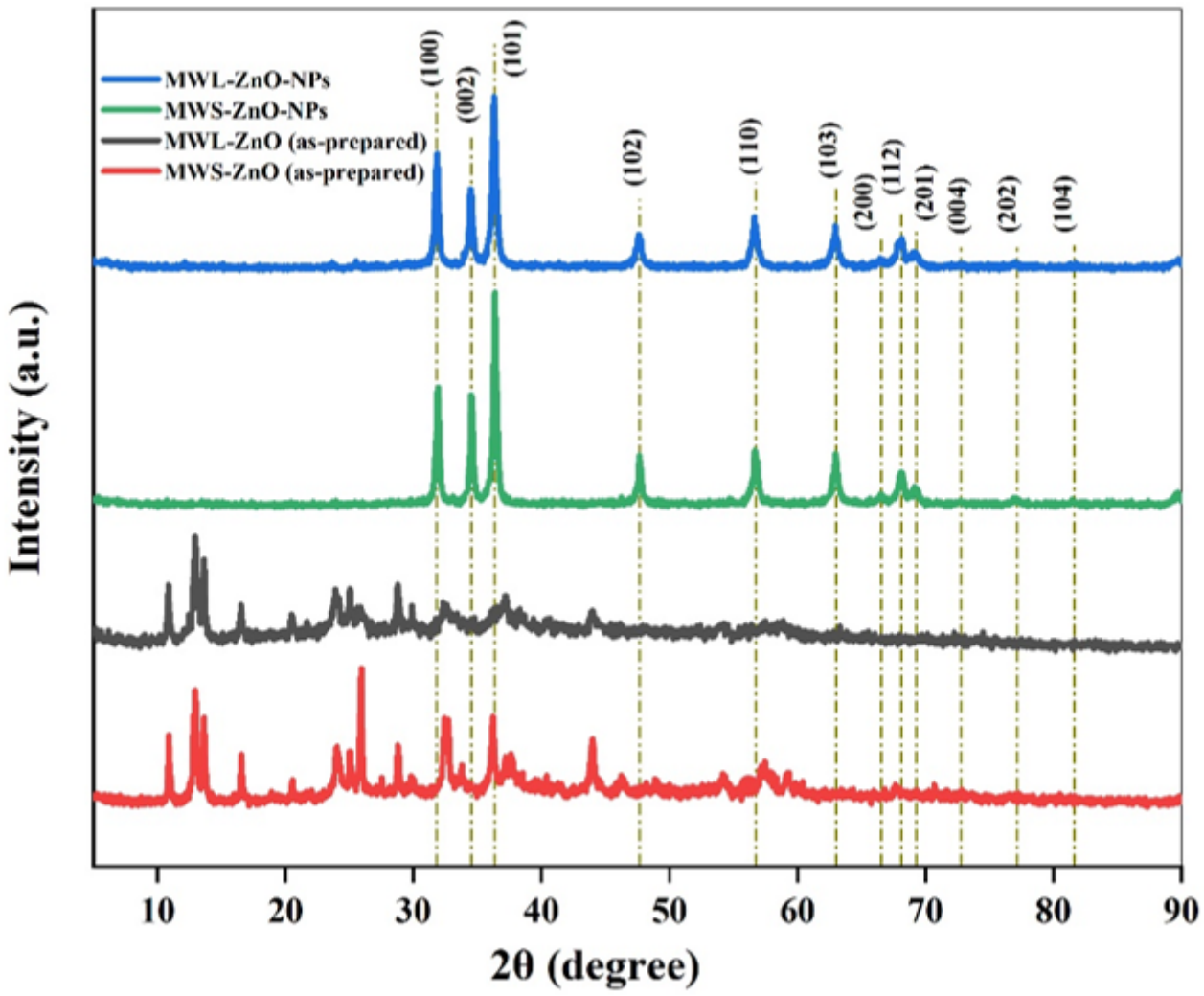

Figure 6

The X-ray diffraction pattern of the as-prepared ZnO samples and ZnO NPs.

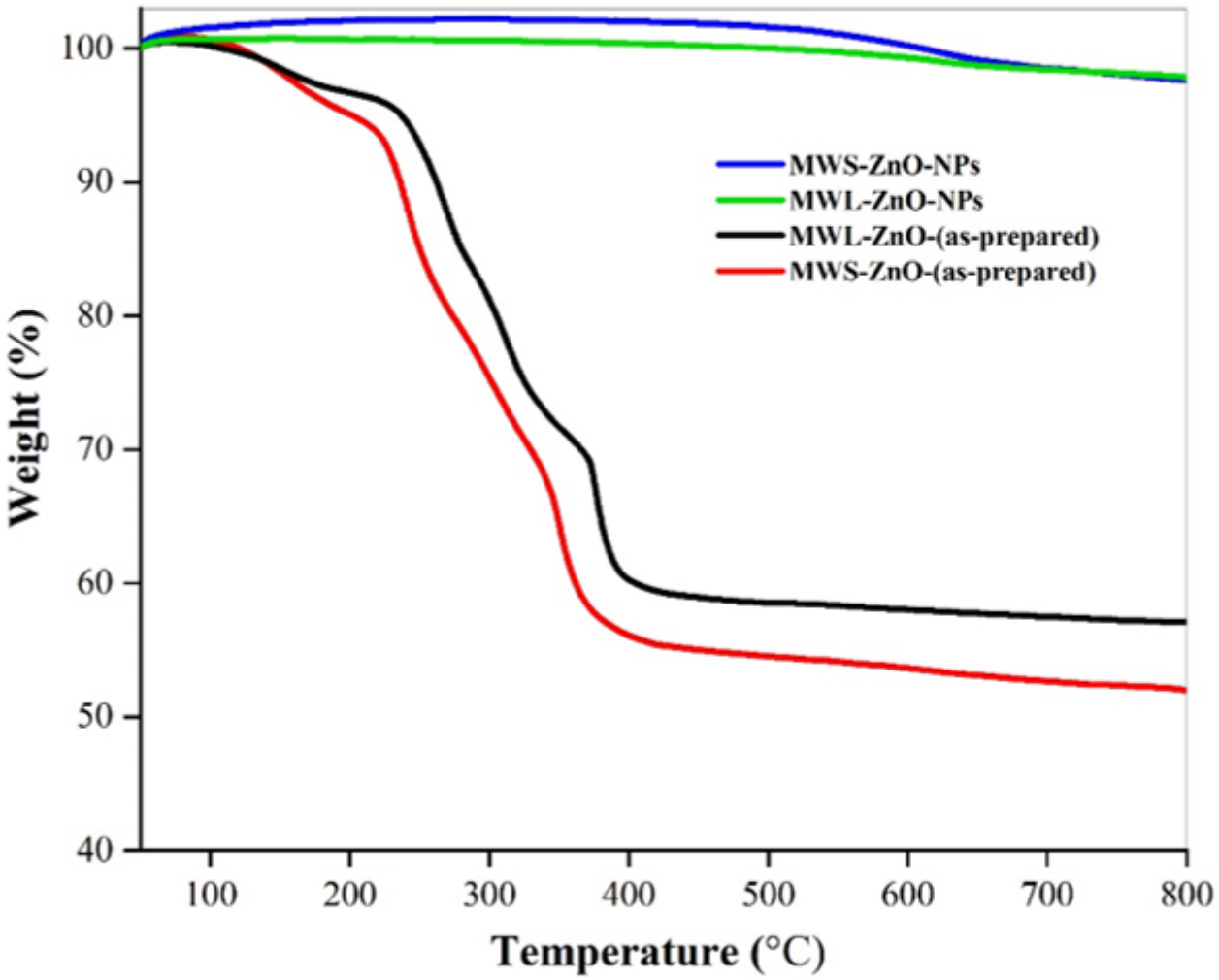

Figure 7

Thermogram (TG) of the as-prepared ZnO and ZnO NPs annealed at 400 °C.

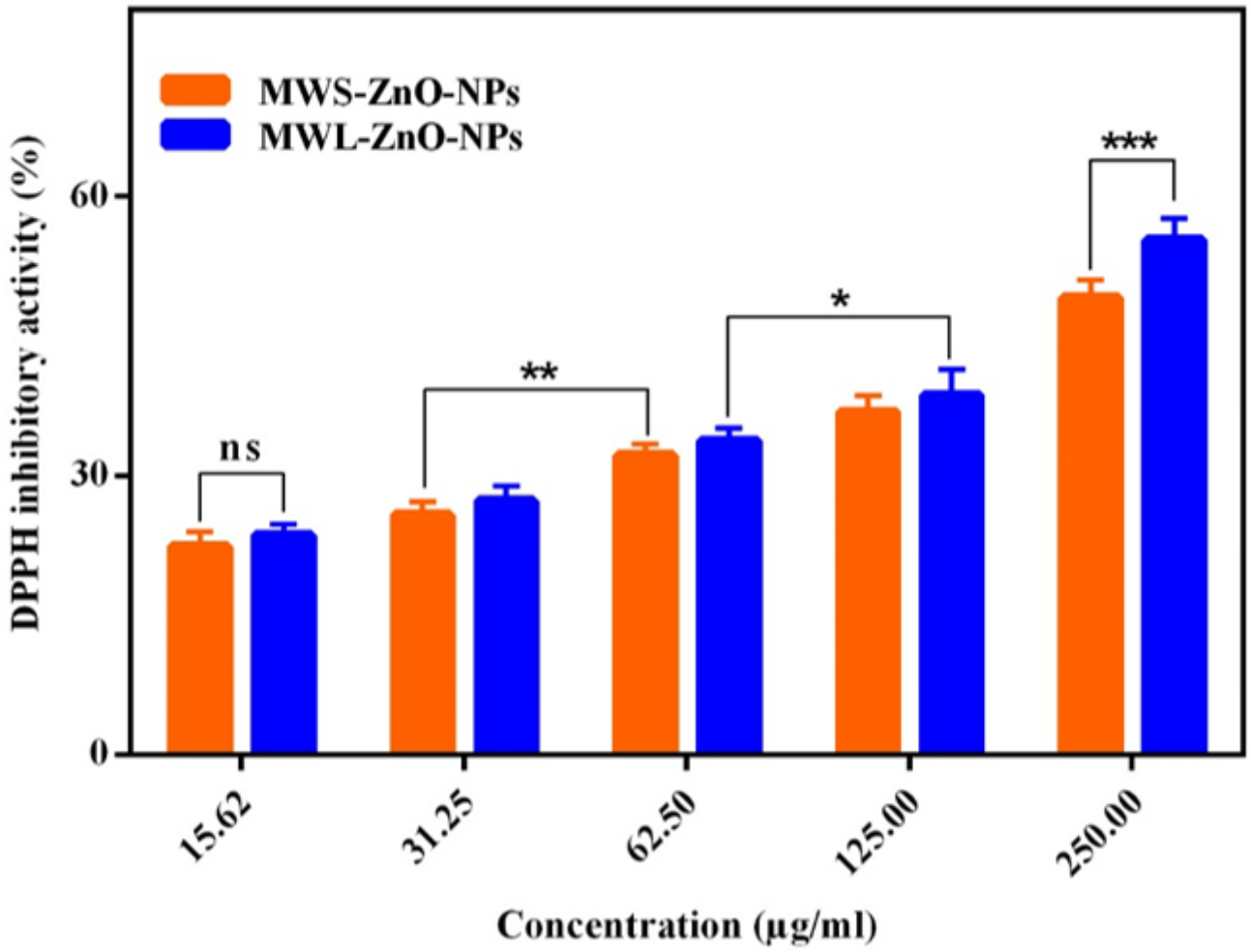

Figure 8

DPPH radical scavenging. (* $p \leq 0.05$, ** $p \leq 0.01$, *** $p \leq 0.001$, and $p \geq 0.05$ considered non-significant).

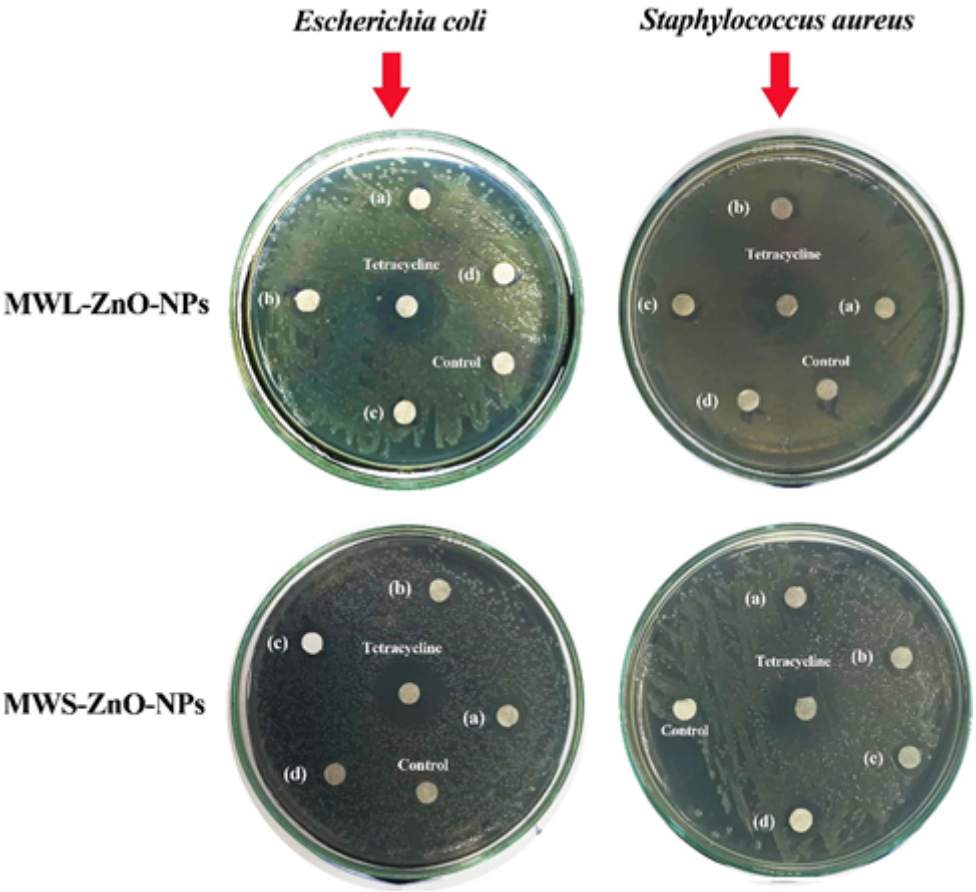

Figure 9

Antibacterial activity of MWL-ZnO-NPs, MWS-ZnO-NPs, and reference antibiotic (tetracycline) against *E. coli* and *S. aureus* (a: 500 µg/mL; b: 250 µg/mL; c: 125 µg/mL and d: 62.5 µg/mL of biosynthesized ZnO NPs).

Supplementary Files

This is a list of supplementary files associated with this preprint. Click to download.

- GraphicalAbstract.png